PNAS
www.pnas.org

Supplementary Information for

Elucidating the G'' overshoot in soft materials with a yield transition via a time-resolved experimental strain decomposition

Gavin J. Donley[a], Piyush K. Singh[a], Abhishek Shetty[b], Simon A. Rogers[a,1]

a: Department of Chemical and Biomolecular Engineering, University of Illinois at Urbana-Champaign
b: Rheology Division, Anton Paar USA

[1]Corresponding Author: Simon A. Rogers
Email: sarogers@illinois.edu

This PDF file includes:

Supplementary text
Figures S1 to S4
Tables S1 to S2
SI References

www.pnas.org/cgi/doi/10.1073/pnas.2003869117

Supplementary Information Text

Material Choice and Preparation. Carbopol 980 was used for this study as a representative polymer microgel as prior literature (1) has suggested that it is a simple yield stress fluid. Xanthan gum was chosen for this study due to its use as the canonical Type III example in (2). Concentrated Ludox colloidal silica was chosen due to its usefulness in comparison to dynamic X-ray scattering studies (3). The filled polymer solution (polyisoprene/squalene/carbon black) was chosen to replicate studies (4, 5) in the filled polymer literature, while being soft enough to measure under 'low' (~50 C) temperatures. The CPCl wormlike micelles were chosen as they are a canonical Type I viscoelastic material (2, 6).

The Carbopol used in this study was prepared as in (7). First, 1 wt% of Carbopol 980 powder (Lubrizol) was dispersed in DI water with a Thinky mixer running at 2000 rpm for 25 minutes followed by 2 minutes of centrifugation at 400 rpm. This was followed by dropwise addition of a 10% NaOH solution (Sigma Aldrich) to neutralize the solution, interspersed with 1 min pulses of 2000 rpm mixing on the Thinky mixer. Once the mixture reached a pH of 5, it was left overnight to equilibrate before testing.

The Xanthan gum solution was prepared as follows: 4 wt% of Xanthan gum (Sigma Aldrich) was dispersed in DI water with a Thinky mixer running at 2000 rpm for 2 hours. The mixture was then stored in a freezer to prevent spoilage. Before loading, the material was thawed with a hotplate set to 50 degrees C for 1 hour, or until the material regained a uniform consistency.

The 55 vol% Ludox used in this study was prepared as in (8). Ludox TM-50 (Sigma Aldrich) was used to fill centrifuge tubes ~45% full. The material was then centrifuged for 1 hour at 12,100 rpm. After pouring off the supernatant, the material was spun down in the centrifuge for another 30 minutes at 12,100 rpm. The volume percentage was ascertained by weighing the supernatant before and after letting the liquid portion evaporate.

The filled polymer solution used in this study was based on the preparation found in (4), with the addition of squalene to allow for measurement at lower temperatures. The formulation utilized polyisoprene (cis, Mw=800,000, PDI=~2.5, Scientific Polymer Products), squalene (Sigma Aldrich), and Carbon Black (from acetylene, Fischer Scientific, finely ground with a mini-grinder) combined in a 2:1:1 mass ratio. The ingredients were then combined with enough hexane (Sigma Aldrich) such that it represented ~90 wt% of the mixture, effectively acting as a co-solvent. 0.1 wt% of BHT (Sigma Aldrich) was also added as an antioxidant. The ingredients were mixed in a sealed flask at 50 C for 24 hours with a stir bar rotating at 300 rpm. Once fully mixed, the hexane was allowed to evaporate in a fume hood overnight, after which the material was left in a vacuum oven at 50 C for 48 hours to ensure all hexane was removed from the system. The resulting rubbery solid was then formed into a layer ~2 mm thick by compressing the sample after heating to 100 C. A circular puck 25 mm in diameter was then formed with a hole punch.

The wormlike micelle solution used in this study was composed of 3.58 wt % of cetylpyridinium chloride (CPCl, Spectrum Laboratory) in a deionized water solution of sodium salicylate (NaSal, Sigma-Aldrich) with a molar ratio of NaSal to CPCl equal to 0.65. The solution was prepared by first adding the desired amount of NaSal to deionized water followed by adding CPCl. All the contents were then shaken inside a bottle and left for at least 2 days for equilibration before rheometric testing.

Rheometer Setup/Geometries Used. The MCR 702 Twindrive rheometer was run in combined motor/transducer mode for all tests using the lower Peltier plate module. The specific rheometer setup for each material tested is shown in table S1. Smooth geometries were utilized for materials which showed negligible wall slip. Materials that showed wall slip used either sandblasted geometries or waterproof sandpaper attached to smooth geometries using double-sided tape, depending on the roughness required. Very stiff materials utilized crosshatched geometries to grip the sample. Temperature and environmental control were achieved via the evaporation blocker attachment. In some cases, additional evaporation protection was provided by either a

barrier of mineral oil around the sample, or by humidifying the air in the evaporation blocker via a water bubbler.

Saramito Model Details. As an example of elastoviscoplastic model in the literature, we have adapted the Saramito model from (9) to a strain separable representation using (10). The form used in our work is:

$$\begin{cases} \frac{1}{G}\dot{\sigma} = \dot{\gamma} + \frac{\eta_s}{G}\ddot{\gamma} \text{ if } \sigma < \sigma_y \\ \tau + \frac{\eta_s+\eta_b}{G}\dot{\tau} = \eta_b\left(\dot{\gamma} + \frac{\eta_s}{G}\ddot{\gamma}\right) \text{ if } \sigma \geq \sigma_y, \text{ where } \tau = \sigma - \sigma_y \end{cases} \quad \text{(S1)}$$

In this form, σ_0 is the yield stress, G is the elastic modulus, η_s is the solid-like damping viscosity, and η_b is the Bingham viscosity above the yield stress. To approximate the Carbopol, these parameters were given the values in table S2.

The model was solved numerically for strain amplitudes $0.00562 \leq \gamma_0 \leq 10$ using MATLAB. The recoverable and unrecoverable strains were calculated as follows:

$$\begin{cases} \dot{\gamma}_{unrec} = 0 \text{ if } \sigma < \sigma_y \\ \dot{\gamma}_{unrec} = \frac{\tau}{\eta_b} = \frac{\sigma-\sigma_y}{\eta_b} \text{ if } \sigma \geq \sigma_y \end{cases} \quad \text{(S2)}$$

$$\dot{\gamma}_{rec} = \dot{\gamma} - \dot{\gamma}_{unrec} \quad \text{(S3)}$$

The resulting LAOS waveforms can be seen in fig. S1.

Inertial Energy Storage and G'_{fluid}. Using similar logic to the definitions of the component moduli from the main manuscript ($G'_{solid}, G''_{solid}, G''_{fluid}$), it is possible to define a component related to fluid-like energy storage as follows:

$$G'_{fluid}(\omega) = \frac{4\left(W_{stored,fluid}(\omega)\right)_{avg}}{{\gamma_0}^2} = \frac{2\left(\gamma_{unrec}(t)\sigma(t)\right)_{avg}}{{\gamma_0}^2} \quad \text{(S4)}$$

In theory, this component should be related to the amount of energy stored inertially in the system (11). The calculated values of G'_{fluid} for each studied material are shown in fig. S2 along with the other component moduli.

At small amplitudes, the contribution of G'_{fluid} to G' is minimal. This makes sense, as inertial energy storage is anticipated to be negligible in the linear regime (11). which clearly reflects elastic deformation as being the primary energy storage mechanism at small amplitudes. Under large deformation amplitudes, the effect of the inertial storage component (G'_{fluid}) increases substantially for the Carbopol, Ludox, and filled polymer solution, accounting for some of the discrepancy between G'_{solid} and G'. The effect is most pronounced for the Carbopol, where $G'_{fluid} > G'_{solid}$ at the largest amplitudes. In the case of the Xanthan gum and worm-like micelles the value of G'_{fluid} remains small over the entire range of amplitudes.

Determination of Viscoplastic Fragility Number. Figure S2 also shows the estimated value of $\Delta G''_{fluid}/G''_{fluid}$ on the left axis of each panel for the entire range of amplitudes tested. Due to the use of a centered difference to calculate $\Delta G''_{fluid}$, the first and last points of each amplitude sweep do not have calculated values. The maximum value of each curve (if positive values are present) is taken as the viscoplastic fragility number (N_{vpf}) described in the text.

Lissajous Figures at Smaller Amplitudes. The Lissajous figures for Carbopol 980 at strain amplitudes $\gamma_0 \leq 0.1$ strain units are shown in fig. S3. The panels of the figure correspond to the panels of fig. 2 in the main manuscript.

Results on Shaving Foam. Additional oscillatory shear/recovery tests were performed on a model foam (Gillette Foamy Regular) (12–14), as an additional example of a type III material. The resulting values of the component moduli are shown in fig. S4, along with the estimation of the viscoplastic fragility number.

When looking at the results from the shaving foam, it is apparent that while the foam shows the same qualitative trends as the other materials, there are substantial quantitative differences between the traditional values from the amplitude sweep and the component moduli. Namely, the component moduli have values that are significantly smaller than the traditional values. We attribute this reduction to the coarsening of the foam (15) which takes place over the ~4-6 hours required to run a single amplitude of the oscillatory shear/recovery.

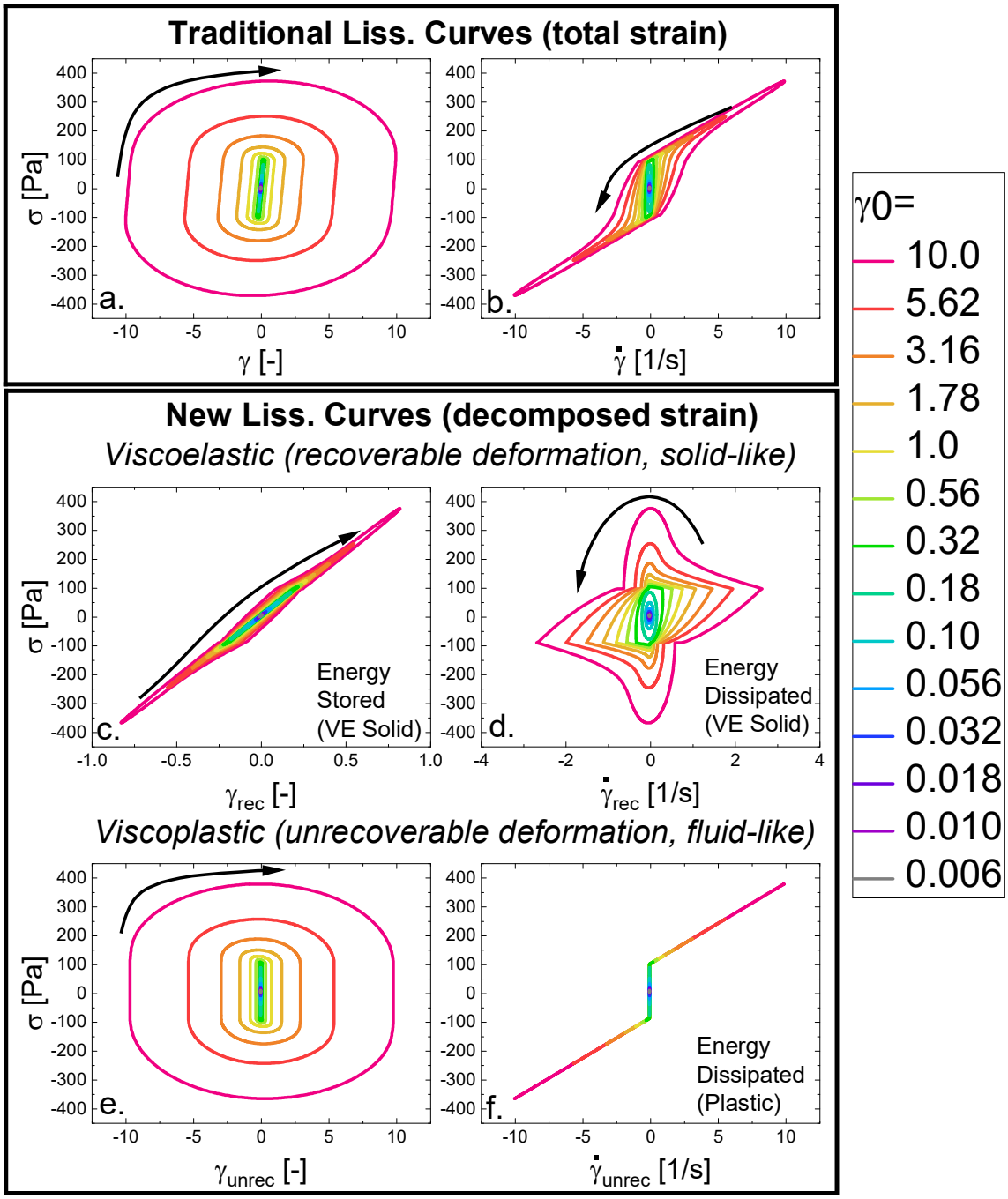

Fig. S1. Lissajous figures containing decomposed strain and strain rate for the Saramito model specified by eqns. S1-S3. (Stress vs.: a. Total Strain, b. Total Rate, c. Recoverable Strain, d. Recoverable Rate, e. Unrecoverable Strain, f. Unrecoverable Rate) The model parameters are found in table S2.

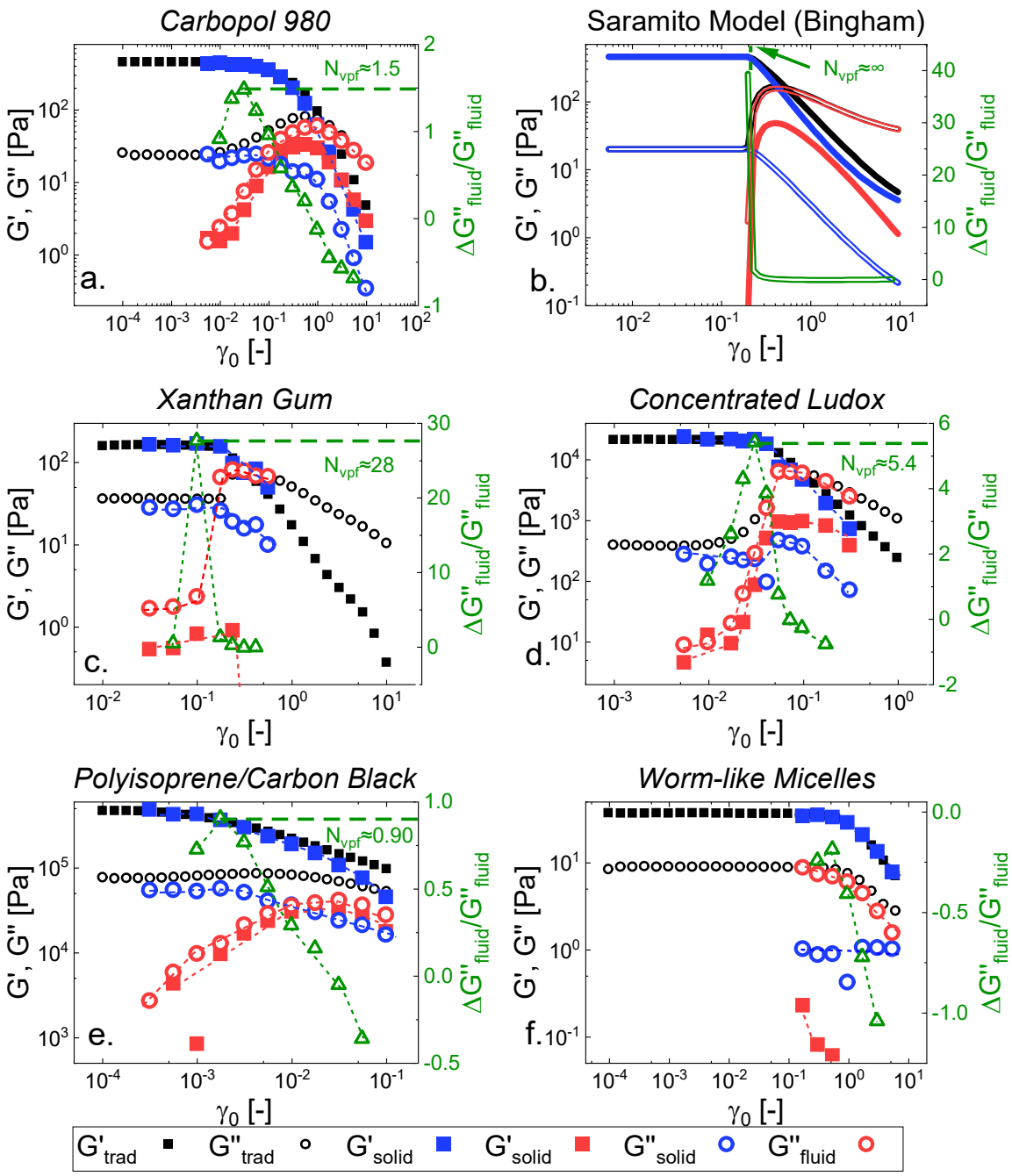

Fig. S2. Decomposed amplitude sweeps for the samples used in this study, including G'_{fluid}. (a. Carbopol, b. Saramito model (Bingham version), c. Xanthan gum, d. Concentrated Ludox, e. Filled polymer, f. Wormlike micelles) The Saramito model parameters are found in table S2. The right axis of each plot also shows the values of $\Delta G''_{fluid}/G''_{fluid}$ relevant to the determination of the viscoplastic fragility number (N_{vpf}).

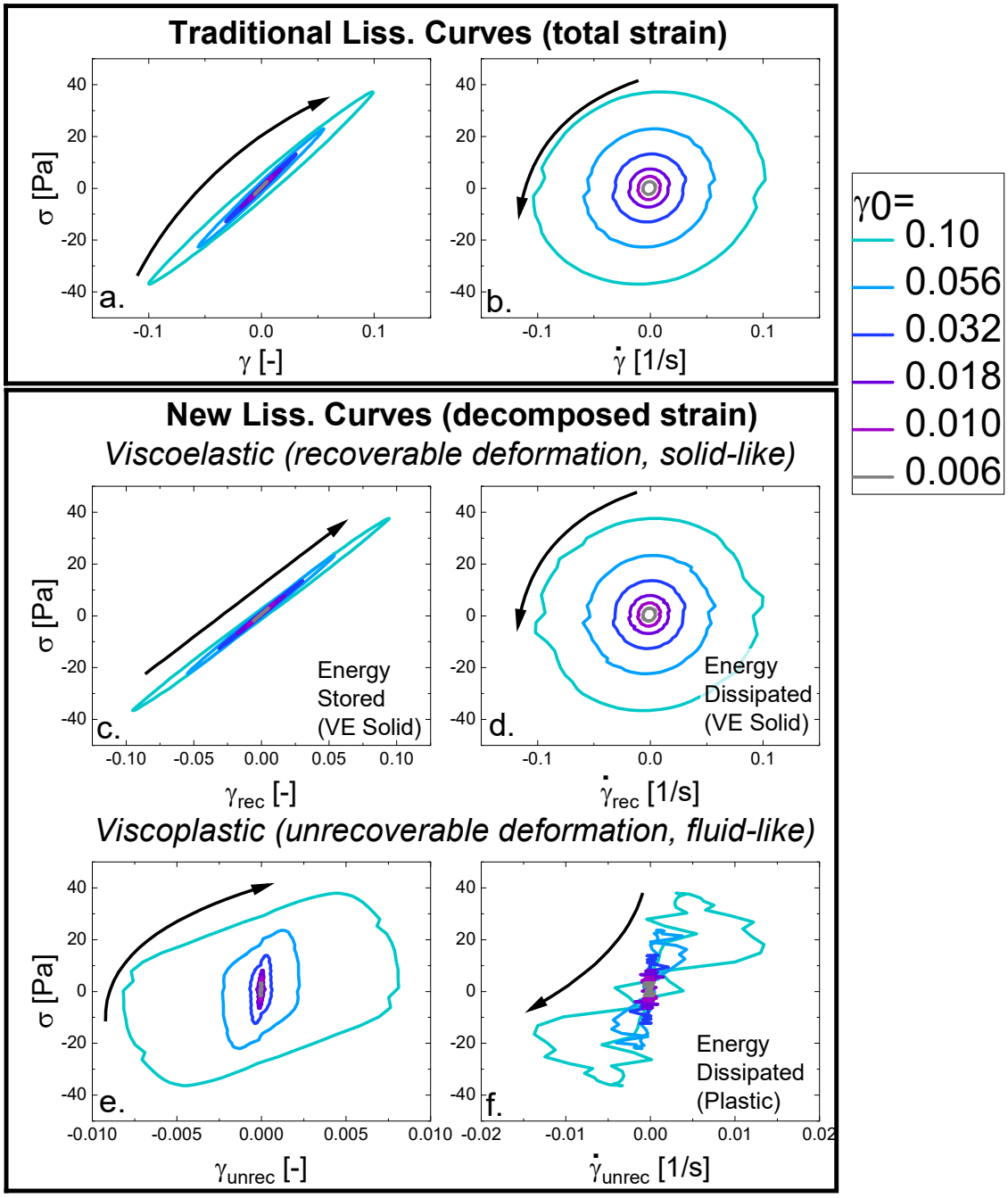

Fig. S3. Lissajous figures containing decomposed strain and strain rate for Carbopol strain at amplitudes strain units (Stress vs.: a. Total Strain, b. Total Rate, c. Recoverable Strain, d. Recoverable Rate, e. Unrecoverable Strain, f. Unrecoverable Rate)

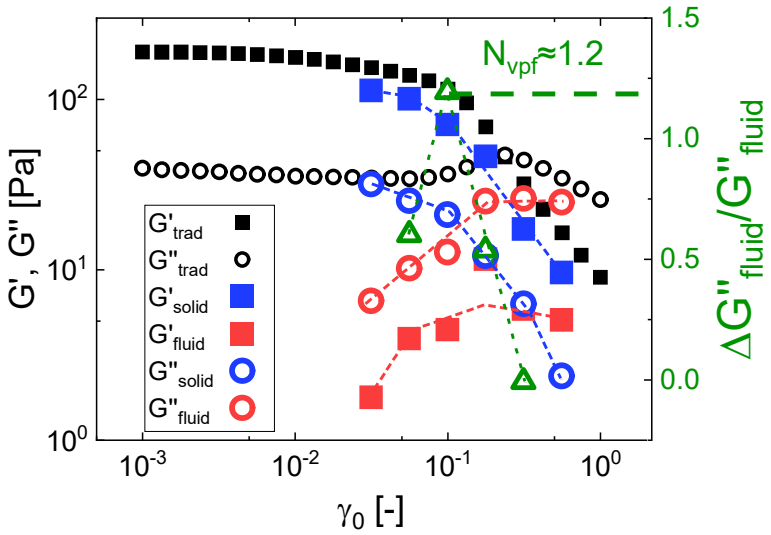

Fig. S4. Decomposed amplitude sweeps and viscoplastic fragility analysis for the Gillette Foamy Regular.

Table S1. Rheometer setup details, including geometry details and other modifications, as well as references from which details were taken.

Material	Geometry	Diameter	Gap	Surface	Temperature	Evaporation Barrier	Ref.
Carbopol 980	parallel plates	50 mm	1 mm	sandpaper, 240 grit	25 C	-	(7)
Xanthan gum	2 deg cone/plate	50 mm	-	smooth	25 C	mineral oil	(2)
Concentrated Ludox	4 deg cone/plate	25 mm	-	smooth	25 C	mineral oil, humidification	(8)
Filled polymer solution	parallel plates	25 mm	2 mm	crosshatched	50 C	-	(4)
Wormlike micelles	2 deg cone/plate	50 mm	-	smooth	23.5 C	-	(6)
Shaving foam	1 deg cone/plate	50 mm	-	sandblasted	25 C	humidification	(12)

Table S2. Parameter selection for the Saramito model.

Parameter	Symbol	Value	Source
Yield stress	σ_{y}	94 Pa	Steady shear flow curve
Elastic modulus	G	460 Pa	Linear regime frequency sweep
Solid damping viscosity	η_{s}	20 Pa*s	Linear regime frequency sweep
Bingham flow viscosity	η_{b}	28 Pa*s	Steady shear flow curve

SI References

1. G. Ovarlez, S. Cohen-Addad, K. Krishan, J. Goyon, P. Coussot, On the existence of a simple yield stress fluid behavior. *J. Nonnewton. Fluid Mech.* **193**, 68–79 (2013).
2. K. Hyun, S. H. Kim, K. H. Ahn, S. J. Lee, Large amplitude oscillatory shear as a way to classify the complex fluids. *J. Nonnewton. Fluid Mech.* **107**, 51–65 (2002).
3. M. C. Rogers, *et al.*, Echoes in x-ray speckles track nanometer-scale plastic events in colloidal gels under shear. *Phys. Rev. E - Stat. Nonlinear, Soft Matter Phys.* **90**, 062310 (2014).
4. X. Fan, *et al.*, Insight into the weak strain overshoot of carbon black filled natural rubber. *Polymer* **167**, 109–117 (2019).
5. A. R. Payne, The dynamic properties of carbon black loaded natural rubber vulcanizates. Part I. *J. Appl. Polym. Sci.* **6**, 57–63 (1962).
6. J. C.-W. Lee, K. M. Weigandt, E. G. Kelley, S. A. Rogers, Structure-Property Relationships via Recovery Rheology in Viscoelastic Materials. *Phys. Rev. Lett.* **122**, 248003 (2019).
7. G. J. Donley, J. R. de Bruyn, G. H. McKinley, S. A. Rogers, Time-resolved dynamics of the yielding transition in soft materials. *J. Nonnewton. Fluid Mech.* **264**, 117–134 (2019).
8. S. A. Rogers, J. D. Park, C. W. J. Lee, Instantaneous dimensionless numbers for transient nonlinear rheology. *Rheol. Acta* **58**, 539–556 (2019).
9. P. Saramito, A new constitutive equation for elastoviscoplastic fluid flows. *J. Nonnewton. Fluid Mech.* **145**, 1–14 (2007).
10. H. A. Barnes, J. F. Hutton, K. Walters, *An introduction to rheology (Vol. 3).* (Elsevier, 1989).
11. N. W. Tschoegl, *The Phenomenological Theory of Linear Viscoelastic Behavior* (Springer Berlin Heidelberg, 1989) https:/doi.org/10.1007/978-3-642-73602-5.
12. F. Rouyer, S. Cohen-Addad, R. Höhler, Is the yield stress of aqueous foam a well-defined quantity? *Colloids Surfaces A Physicochem. Eng. Asp.* **263**, 111–116 (2005).
13. M. Dinkgreve, J. Paredes, M. M. Denn, D. Bonn, On different ways of measuring “the” yield stress. *J. Nonnewton. Fluid Mech.* **238**, 233–241 (2016).
14. A. Saint-Jalmes, D. J. Durian, Vanishing elasticity for wet foams: Equivalence with emulsions and role of polydispersity. *J. Rheol.* **43**, 1411–1422 (1999).
15. S. Cohen-Addad, H. Hoballah, R. Höhler, Viscoelastic response of a coarsening foam. *Phys. Rev. E - Stat. Physics, Plasmas, Fluids, Relat. Interdiscip. Top.* **57**, 6897 (1998).